DOI: 10.11844/cjcb.2026.03.0015
中国细胞生物学学报 Chinese Journal of Cell Biology 2026, 48(3): 737–746 CSTR: 32200.14.cjcb.2026.03.0015

miR-200a-3p靶向调节ALKBH5对碱烧伤小鼠角膜新生血管的影响

张嘉声[1] 林珊[2]* 刘诗亮[3]
([1]武汉市第一医院眼科, 武汉 430030; [2]华中科技大学同济医学院附属梨园医院儿科, 武汉 430077;
[3]华中科技大学同济医学院附属梨园医院眼科, 武汉 430077)

摘要 该研究旨在探讨微小RNA(miR)-200a-3p靶向调节RNA去甲基化酶AlkB同源物5(ALKBH5)对碱烧伤小鼠角膜新生血管的影响。将108只小鼠分为control组、alkali burn组、AAV-NC组、AAV-pre-miR-200a-3p组、AAV-pre-miR-200a-3p+pc-NC组、AAV-pre-miR-200a-3p+pc-ALKBH5组, 每组18只, 除control组外, 其余组小鼠均使用浸于1 mol/L NaOH的滤纸进行角膜碱烧伤模型构建。由眼科医生盲法评估角膜混浊程度; 苏木素–伊红(HE)染色评估角膜组织病理学变化; 马松(Masson)三色染色评估胶原沉积情况; TUNEL染色检测凋亡情况; 免疫荧光染色检测血小板–内皮细胞黏附分子(CD31)表达情况; 实时荧光定量逆转录PCR(RT-qPCR)检测miR-200a-3p水平; Western blot检测ALKBH5蛋白表达情况; 双荧光素酶报告基因和RIP实验测定miR-200a-3p与*ALKBH5*的靶向关系。结果显示, 与control组相比, alkali burn组小鼠角膜混浊评分提高, 角膜基质炎症细胞浸润, 基质胶原结构松弛, 角膜厚度增加, 胶原体积分数、角膜细胞凋亡率、CD31相对荧光强度及ALKBH5蛋白表达水平均提高, miR-200a-3p表达水平降低(P<0.05); 与AAV-NC组相比, AAV-pre-miR-200a-3p组小鼠角膜混浊评分降低, 角膜厚度减少, 胶原体积分数、角膜细胞凋亡率、CD31相对荧光强度及ALKBH5蛋白表达水平降低, miR-200a-3p表达水平提高(P<0.05); 与AAV-pre-miR-200a-3p+pc-NC组相比, AAV-pre-miR-200a-3p+pc-ALKBH5组小鼠角膜混浊评分提高, 角膜厚度增加, 胶原体积分数、角膜细胞凋亡率、CD31相对荧光强度及ALKBH5蛋白表达水平提高(P<0.05); 双荧光素酶活性结果显示, miR-200a-3p与*ALKBH5*存在靶向关系(P<0.05)。总结得出, miR-200a-3p通过抑制ALKBH5表达抑制碱烧伤小鼠的角膜新生血管生成。

关键词 微小RNA-200a-3p; RNA去甲基化酶AlkB同源物5; 碱烧伤小鼠; 角膜新生血管

The Effect of miR-200a-3p on Corneal Neovascularization in Alkali Burned Mice by Targeting and Regulating ALKBH5

ZHANG Jiasheng[1], LIN Shan[2]*, LIU Shiliang[3]
([1]*Department of Ophthalmology, Wuhan No.1 Hospital, Wuhan 430030, China*; [2]*Department of Pediatrics, Liyuan Hospital of Tongji Medical College of Huazhong University of Science & Technology, Wuhan 430077, China*; [3]*Department of Ophthalmology, Liyuan Hospital of Tongji medical College of Huazhong University of Science & Technology, Wuhan 430077, China*)

Abstract This study aimed to explore the effect of miR (microRNA)-200a-3p on corneal neovascularization in alkali burned mice by targeting and regulating ALKBH5 (RNA demethylase AlkB homologue 5). Totally 108 mice

收稿日期: 2025-12-16 接受日期: 2026-01-08
湖北省自然科学基金(批准号: 2024AFB122)资助的课题
*通信作者。Tel: 15802779086, E-mail: whlyhospitaldoctor@126.com
Received: December 16, 2025 Accepted: January 8, 2026
This work was supported by the Natural Science Foundation of Hubei Province (Grant No.2024AFB122)
*Corresponding author. Tel: +86-15802779086, E-mail: whlyhospitaldoctor@126.com

were assigned into the control group, the alkali burn group, the AAV-NC group, the AAV-pre-miR-200a-3p group, the AAV-pre-miR-200a-3p+pc-NC group, and the AAV-pre-miR-200a-3p+pc-ALKBH5 group, with 18 per group. Except for the control group, the mice in the other groups were all used to construct corneal alkali burn models with filter paper soaked in 1 mol/L NaOH. Corneal opacity was blind assessed by ophthalmologist. The histopathological changes of corneal tissue was evaluated by HE staining. Collagen deposition was evaluated by Masson tricolor staining. Apoptosis was measured by TUNEL staining. The expression of CD31 (platelet-endothelial cell adhesion molecule) was measured by immunofluorescence staining. The level of miR-200a-3p was detected by RT-qPCR (real-time reverse transcription PCR). The expression of ALKBH5 protein was detected by Western blot. In addition, the targeting relationship between miR-200a-3p and *ALKBH5* was determinethed by dual-luciferase reporter gene and RIP experiment. The results showed that compared with the control group, the corneal opacity score of mice in the alkali burn group raised, the inflammatory cells infiltrated the corneal stroma, the collagen structure of the stroma relaxed, and the corneal thickness raised. The collagen volume fraction, corneal apoptosis rate, relative fluorescence intensity of CD31 and protein expression of ALKBH5 all increased, while the expression of miR-200a-3p declined ($P<0.05$). Compared with the AAV-NC group, the corneal opacity score of mice in the AAV-pre-miR-200a-3p group declined, the corneal thickness declined, the collagen volume fraction, corneal apoptosis rate, relative fluorescence intensity of CD31 and protein expression of ALKBH5 declined, while the expression of miR-200a-3p raised ($P<0.05$). Compared with the AAV-pre-miR-200a-3p+pc-NC group, the corneal opacity score and corneal thickness of mice in the AAV-pre-miR-200a-3p+pc-ALKBH5 group increased, the collagen volume fraction, corneal cell apoptosis rate, relative fluorescence intensity of CD31 and protein expression of ALKBH5 raised ($P<0.05$). The results of dual-luciferase activity and RIP experiment showed that miR-200a-3p had a targeting relationship with *ALKBH5* ($P<0.05$). In conclusion, miR-200a-3p inhibits corneal neovascularization in alkali burned mice by suppressing the expression of ALKBH5.

Keywords microRNA-200a-3p; RNA demethylase AlkB homologue 5; alkali burned mice; corneal neovascularization

角膜是一种透明的无血管组织, 角膜碱烧伤是一种常见的眼部损伤类型, 临床上难以治疗[1]。碱烧伤后的角膜新生血管形成是一种严重的并发症, 它不仅严重影响患者的视力, 而且是角膜移植失败的主要原因。角膜新生血管形成每年影响约140万患者[2]。角膜新生血管形成会引发角膜混浊, 其特征是从角膜缘向其透明核心形成新血管。同时, 角膜新生血管形成诱导的角膜水肿会降低角膜透明度并对视力产生不利影响[3]。微小RNA(microRNA, miRNA)是保守的、短的、非编码RNA, 在调节基因表达中具有至关重要的作用。近期证据表明, miRNA密切参与各种角膜疾病的病理生理学, 尤其是在调节角膜伤口愈合、炎症和新生血管形成方面发挥着至关重要的调控作用[4]。已有研究表明, 多种miRNA可通过调节血管内皮生长因子(vascular endothelial growth factor, VEGF)和血管生成在角膜新生血管形成中发挥作用[5]; miR-200-3p通过阻断转化生长因子-β2(transforming growth factor-β2, TGF-β2)/Smad通路抑制糖尿病视网膜病变的细胞增殖并减少细胞死亡[6]。RNA去甲基化酶AlkB同源物5(RNA demethylase AlkB homolog 5, ALKBH5)是参与调节N^6-甲基腺苷(N^6-methyladenosine, m^6A)修饰的去甲基化酶之一。除在RNA m^6A修饰的动态调控中发挥作用外, 近年来发现ALKBH5在各种组织纤维化过程中也发挥着重要作用[7]。已有研究表明, ALKBH5通过介导叉头框蛋白M1(forkhead box M1, FOXM1) m^6A去甲基化调节角膜新生血管形成[8]。此外, Starbase数据库显示miR-200a-3p与*ALKBH5*存在互补序列, 但尚未有研究将miR-200a-3p与*ALKBH5*关联验证其在角膜新生血管形成中的作用, 因此, 本研究采用角膜碱烧伤小鼠模型, 首次探究miR-200a-3p靶向*ALKBH5*调控角膜新生血管形成的全新机制。

1 材料与方法

1.1 动物与细胞

108只雄性C57BL/6小鼠(8周龄, 20~24 g)购

于无锡恒泰实验动物养殖有限公司, 生产许可证号: SCXK(苏) 2025-0003, 室温为22~24 ℃, 湿度为45%~50%, 光/暗循环为12 h, 自由获得食物与水, 进行一周适应性喂养, 本研究所有动物实验均经武汉市第一医院实验动物伦理委员会审核并批准(批准号: 2024-013)。

人脐静脉血管内皮细胞(human umbilical vein endothelial cell, HUVEC)(STM-CL-5186)购自思泰默(上海)生物科技有限公司, 内皮细胞专用培养基培养, 培养箱设置为95%空气、5%二氧化碳、37 ℃, 湿度为70%~80%。

1.2 主要试剂

AAV-miR-200a-3p、AAV-NC、AAV-pcDNA-ALKBH5和AAV-pcDNA-NC购自通用生物(安徽)股份有限公司; 苏木素–伊红(HE)染色试剂盒(货号: E607318-0200)、RNA结合蛋白免疫沉淀(RIP)试剂盒(货号: B605109)购自生工生物工程(上海)股份有限公司; Masson三色染色试剂盒(货号: BP-DL021)购自南京森贝伽生物科技有限公司; TUNEL凋亡检测试剂盒(红色荧光, 货号: PF00009)购自武汉三鹰生物技术有限公司; 增强型ECL化学发光试剂盒(货号: BF06053)购自苏州博奥龙科技有限公司; miRNA逆转录专用试剂盒(货号: MR101)购自南京诺唯赞生物科技股份有限公司; SYBR Premix Ex Taq(货号: RR420A)购自北京智杰方远科技有限公司; 血小板−内皮细胞黏附分子(CD31)抗体(货号: ab222783)、山羊抗兔IgG二抗(偶联488, 货号: ab150077)、ALKBH5兔单克隆抗体(货号: ab195377)、GAPDH兔单克隆抗体(货号: ab181603)、HRP标记的羊抗兔IgG抗体(货号: ab6721)购于英国Abcam公司。

1.3 实验方法

1.3.1 碱烧伤小鼠模型构建及分组转染 因小鼠角膜属于眼表微小组织, 体积较小, 根据实验和统计学效力需求设置样本量为18, 将108只小鼠数字法随机分为control组、alkali burn组、AAV-NC组、AAV-pre-miR-200a-3p组、AAV-pre-miR-200a-3p+pc-NC组、AAV-pre-miR-200a-3p+pc-ALKBH5组, 每组18只, 除control组外, 其余组小鼠均进行碱烧伤模型构建[8]: 先腹腔注射氯胺酮(70 mg/kg)和右美托咪定(0.25 mg/kg)进行麻醉, 眼部滴盐酸丙美卡因滴眼液, 将浸泡在1 mol/L NaOH中的直径为2 mm的圆形滤纸放置在右角膜中央40 s, 引起碱灼伤, 然后用生理盐水冲洗右侧角膜1 min, 随后, 小鼠每天2次使用氧氟沙星滴眼液, 持续3天, 以防止感染[9]。造模结束后, AAV-NC组、AAV-pre-miR-200a-3p组、AAV-pre-miR-200a-3p+pc-NC组、AAV-pre-miR-200a-3p+pc-ALKBH5组小鼠分别尾静脉注射含AAV-NC、AAV-miR-200a-3p、AAV-miR-200a-3p和AAV-pcDNA-NC、AAV-miR-200a-3p和AAV-pcDNA-ALKBH5的病毒悬液, 7天后, 通过腹腔注射过量戊巴比妥钠(150 mg/kg)杀死小鼠, 然后将其右眼球迅速转移到冰床上剥离角膜。

1.3.2 实时荧光定量逆转录PCR(RT-qPCR)检测miR-200a-3p 使用TRIzol试剂提取角膜组织总RNA, 使用miRNA逆转录专用试剂盒将RNA逆转为cDNA, 使用SYBR Premix Ex Taq进行RT-qPCR反应, 记录Ct值, 并采用熔解曲线验证扩增特异性, 基因扩增产物的熔解曲线呈单一尖锐峰, 无杂峰、无宽峰, 表明引物特异性良好, 最后, 使用$2^{-\Delta\Delta Ct}$法计算miR-200a-3p水平。引物序列如下。miR-200a-3p正向引物为5′-GGC TAA CAC TGT CTG GTA ACG ATG-3′, 反向引物为5′-GTG CAG GGT CCG AGG T-3′; *U6*正向引物为5′-CAA ATT CGT GAA GCG TTC CAT AT-3′, 反向引物为5′-GCT TCA CGA ATT TGC GTG TCA TCC TTG C-3′。

1.3.3 角膜混浊评估 各组小鼠处理7天后, 小心地将右眼角膜与眼球分离, 同时避免角膜组织以及眼球内部结构的损伤, 分离后的右眼角膜在1× PBS中清洗。由对分组不知情的眼科医生进行分级评分, 角膜混浊分级如下: 0, 完全透明; 1, 轻度基质混浊, 虹膜清晰可见; 2, 中度基质混浊, 虹膜隐约可见; 3, 角膜混浊严重, 虹膜隐约可见; 4, 不透明角膜, 虹膜不可见[10]。

1.3.4 HE染色评估角膜组织病理学变化 将角膜组织使用4%多聚甲醛4 ℃固定24 h后, 包埋于石蜡, 并制成切片。随后, 用苏木素染液染细胞核, 室温孵育8 min, 用伊红染色液复染1 min, 用显微镜进行观察。

1.3.5 Masson三色染色评估胶原沉积 角膜组织的石蜡切片常规脱蜡至水, 按照试剂盒说明进行Masson三色染色以评估胶原蛋白沉积情况。角膜纤维化程度按以下公式确定: 胶原体积分数=胶原蛋白面积/总面积×100%。

1.3.6 TUNEL染色检测凋亡 角膜组织石蜡切片用二甲苯脱蜡, 然后经梯度(100%、95%、85%、

75%)乙醇复水, 蛋白酶K(proteinase K)溶液室温孵育20 min, PBS浸润清洗, 加入50 μL TUNEL反应混合液, 37 ℃避光孵育2 h, 清洗后用DAPI室温避光复染10 min。用荧光显微镜观察, TUNEL阳性细胞百分比为凋亡率。

1.3.7 CD31免疫荧光染色 将角膜组织冷冻制成切片后, 室温平衡10~20 min, 然后, 用4%多聚甲醛4 ℃固定15 min。用含有0.2% Triton X-100的即用型山羊血清封闭2 h, 之后与CD31抗体(稀释比1:100)在4 ℃下孵育过夜, 然后与荧光二抗(稀释比1:1 000)在室温下避光孵育1 h。利用DAPI对细胞核进行染色, 并在荧光显微镜下观察。

1.3.8 Western blot检测ALKBH5蛋白表达情况 使用RIPA裂解液从角膜中提取总蛋白。将等量的蛋白(20 μg)在聚丙烯酰胺凝胶中分离并转移到PVDF膜上, 然后在5%脱脂牛奶中室温封闭1 h。随后, 将膜与ALKBH5(稀释比1:5 000)、GAPDH一抗(稀释比1:10 000)在4 ℃下孵育过夜, 再与相应二抗(稀释比1:5 000)室温下孵育1 h。最后, 使用增强型ECL化学发光试剂盒显色并通过ImageJ软件进行分析。

1.3.9 双荧光素酶报告基因测定 利用荧光素酶报告基因载体构建*ALKBH5*野生型(WT)或突变型(MUT)质粒, 并使用Lipofectamine 2000将其分别与miR-NC、miR-200a-3p mimic质粒共转染至HUVEC, 随后, 将细胞于37 ℃孵育48 h, 然后使用双荧光素酶报告基因检测试剂盒测定荧光素酶活性, 计算萤火虫荧光素酶与海肾荧光素酶的发光比。

1.3.10 RIP实验验证miR-200a-3p与*ALKBH5*的靶向关系 将细胞接种于6孔板, 培养至密度达80%~90%时用RIP裂解液, 冰上裂解30 min, 超声破碎, 4 ℃、12 000 r/min离心15 min, 收集上清液, 使用Ago2抗体和IgG抗体进行免疫沉淀, 用磁珠捕获抗体−蛋白-RNA复合物, 提取总RNA。采用RT-qPCR检测miR-200a-3p和*ALKBH5*的表达水平。

1.4 统计学分析

实验数据用($\bar{x}\pm s$)表示, 采用GraphPad Prism 7.0软件进行统计分析, 数据均符合正态分布, 符合方差齐性检验的多组数据进行单因素方差分析, 进一步两组间比较采用*t*检验, 多组间比较采用单因素方差分析和Tukey's多重检验。$P<0.05$代表有统计学差异。

2 结果

2.1 各组小鼠角膜中miR-200a-3p水平比较

与control组相比, alkali burn组小鼠角膜miR-200a-3p水平降低($P<0.05$); 与AAV-NC组相比, AAV-pre-miR-200a-3p组小鼠角膜miR-200a-3p水平提高($P<0.05$); 与AAV-pre-miR-200a-3p+pc-NC组相比, AAV-pre-miR-200a-3p+pc-ALKBH5组小鼠角膜miR-200a-3p水平降低($P<0.05$); 见表1。

2.2 各组小鼠角膜混浊评估比较

与control组相比, alkali burn组小鼠角膜混浊评分提高($P<0.05$); 与AAV-NC组相比, AAV-pre-miR-200a-3p组小鼠角膜混浊评分降低($P<0.05$); 与AAV-pre-miR-200a-3p+pc-NC组相比, AAV-pre-miR-200a-3p+pc-ALKBH5组小鼠角膜混浊评分提高($P<0.05$); 见表2。

2.3 各组小鼠角膜HE染色比较

与control组相比, alkali burn组小鼠角膜基质炎症细胞浸润, 基质胶原结构松弛, 角膜厚度增加

表1 各组小鼠角膜中miR-200a-3p水平比较

Table 1 Comparison of miR-200a-3p levels in the cornea of mice in each group

分组 Groups	miR-200a-3p
Control	1.04±0.11
Alkali burn	0.53±0.06*
AAV-NC	0.55±0.07
AAV-pre-miR-200a-3p	0.98±0.12#
AAV-pre-miR-200a-3p+pc-NC	0.99±0.13
AAV-pre-miR-200a-3p+pc-ALKBH5	0.59±0.08&
F	112.335
P	0.000

*$P<0.05$, 与control组比较; #$P<0.05$, 与AAV-NC组比较; &$P<0.05$, 与AAV-pre-miR-200a-3p+pc-NC组比较。$\bar{x}\pm s$, $n=18$。

*$P<0.05$ compared with control group; #$P<0.05$ compared with AAV-NC group; &$P<0.05$ compared with AAV-pre-miR-200a-3p+pc-NC group. $\bar{x}\pm s$, $n=18$.

表2 各组小鼠角膜混浊评分比较

Table 2 Comparison of corneal opacity scores of mice in each group

分组 Groups	角膜混浊评分 Corneal opacity score
Control	0.09±0.01
Alkali burn	2.89±0.32*
AAV-NC	2.92±0.34
AAV-pre-miR-200a-3p	1.47±0.17#
AAV-pre-miR-200a-3p+pc-NC	1.45±0.16
AAV-pre-miR-200a-3p+pc-ALKBH5	2.74±0.31&
F	374.080
P	0.000

*P<0.05, 与control组比较; #P<0.05, 与AAV-NC组比较; &P<0.05, 与AAV-pre-miR-200a-3p+pc-NC组比较。$\bar{x}\pm s$, n=18。

*P<0.05 compared with control group; #P<0.05 compared with AAV-NC group; &P<0.05 compared with AAV-pre-miR-200a-3p+pc-NC group. $\bar{x}\pm s$, n=18.

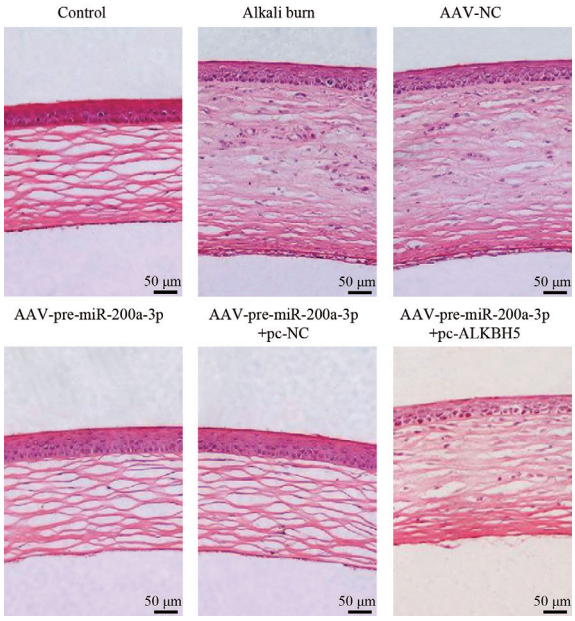

图1 各组小鼠角膜HE染色

Fig.1 HE staining of mouse cornea in each group

(P<0.05); 与AAV-NC组相比, AAV-pre-miR-200a-3p组小鼠角膜炎症细胞浸润减少, 结构更加紧密, 角膜厚度减少(P<0.05); 与AAV-pre-miR-200a-3p+pc-NC组相比, AAV-pre-miR-200a-3p+pc-ALKBH5组小鼠基质炎症细胞浸润增加, 基质胶原结构松弛, 角膜厚度增加(P<0.05); 见图1与表3。

2.4 各组小鼠角膜胶原沉积情况比较

与control组相比, alkali burn组小鼠角膜胶原体积分数提高(P<0.05); 与AAV-NC组相比, AAV-pre-miR-200a-3p组小鼠角膜胶原体积分数降低(P<0.05); 与AAV-pre-miR-200a-3p+pc-NC组相比, AAV-pre-miR-200a-3p+pc-ALKBH5组小鼠角膜胶原体积分数提高(P<0.05); 见图2与表4。

2.5 各组小鼠角膜细胞凋亡情况比较

与control组相比, alkali burn组小鼠角膜细胞凋亡率提高(P<0.05); 与AAV-NC组相比, AAV-pre-miR-200a-3p组小鼠角膜细胞凋亡率降低(P<0.05); 与AAV-pre-miR-200a-3p+pc-NC组相比, AAV-pre-miR-200a-3p+pc-ALKBH5组小鼠角膜细胞凋亡率提高(P<0.05); 见图3与表5。

2.6 各组小鼠角膜CD31免疫荧光染色比较

与control组相比, alkali burn组小鼠角膜CD31相对荧光强度提高(P<0.05); 与AAV-NC组相比, AAV-pre-miR-200a-3p组小鼠角膜CD31相对荧光强度降

表3 各组小鼠平均角膜厚度比较

Table 3 Comparison of average corneal thickness of mice in each group

分组 Groups	平均角膜厚度/μm Average corneal thickness /μm
Control	261.58±28.59
Alkali burn	396.96±42.75*
AAV-NC	395.38±42.19
AAV-pre-miR-200a-3p	291.47±31.48#
AAV-pre-miR-200a-3p+pc-NC	292.84±32.25
AAV-pre-miR-200a-3p+pc-ALKBH5	375.96±39.58&
F	16.354
P	0.000

*P<0.05, 与control组比较; #P<0.05, 与AAV-NC组比较; &P<0.05, 与AAV-pre-miR-200a-3p+pc-NC组比较。$\bar{x}\pm s$, n=18。

*P<0.05 compared with control group; #P<0.05 compared with AAV-NC group; &P<0.05 compared with AAV-pre-miR-200a-3p+pc-NC group. $\bar{x}\pm s$, n=18.

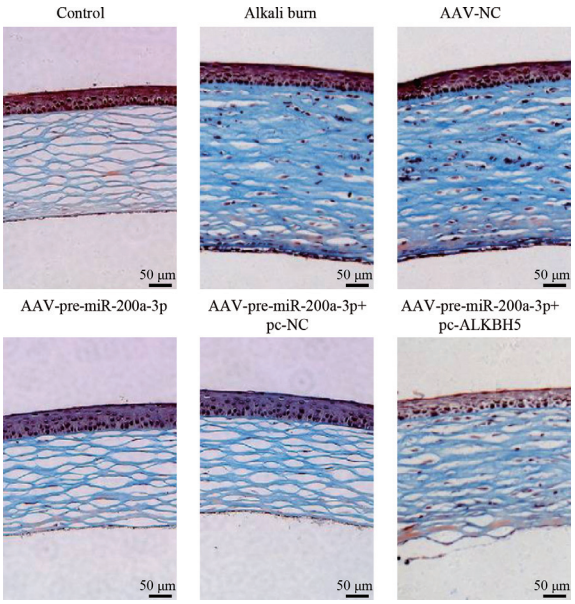

图2 各组小鼠角膜Masson三色染色

Fig.2 Masson's trichrome staining of mouse corneas in each group

表4 各组小鼠角膜胶原体积分数比较

Table 4 Comparison of corneal collagen volume fraction of mice in each group

分组 Groups	胶原体积分数/% Collagen volume fraction /%
Control	48.36±5.58
Alkali burn	67.82±7.94*
AAV-NC	68.33±7.38
AAV-pre-miR-200a-3p	53.29±5.74#
AAV-pre-miR-200a-3p+pc-NC	52.75±6.12
AAV-pre-miR-200a-3p+pc-ALKBH5	65.83±7.25&
F	10.482
P	0.000

*P<0.05, 与control组比较; #P<0.05, 与AAV-NC组比较; &P<0.05, 与AAV-pre-miR-200a-3p+pc-NC组比较。$\bar{x}\pm s$, n=18。

*P<0.05 compared with control group; #P<0.05 compared with AAV-NC group; &P<0.05 compared with AAV-pre-miR-200a-3p+pc-NC group. $\bar{x}\pm s$, n=18.

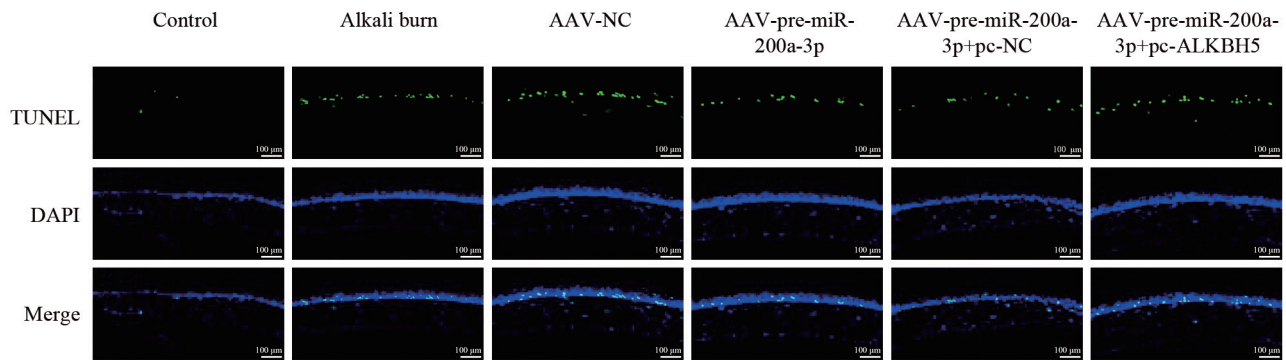

图3 各组小鼠角膜TUNEL染色

Fig.3 TUNEL staining of mouse cornea in each group

表5 各组小鼠角膜细胞凋亡率比较

Table 5 Comparison of corneal cell apoptosis rates in each group of mice

分组 Groups	凋亡率/% Apoptosis rate /%
Control	1.02±0.11
Alkali burn	24.74±2.82*
AAV-NC	25.18±2.97
AAV-pre-miR-200a-3p	12.46±1.58$^{\#}$
AAV-pre-miR-200a-3p+pc-NC	13.25±1.61
AAV-pre-miR-200a-3p+pc-ALKBH5	22.17±2.63$^{\&}$
F	110.509
P	0.000

*P<0.05, 与control组比较; $^{\#}P$<0.05, 与AAV-NC组比较; $^{\&}P$<0.05, 与AAV-pre-miR-200a-3p+pc-NC组比较。$\bar{x}\pm s$, n=18。

*P<0.05 compared with control group; $^{\#}P$<0.05 compared with AAV-NC group; $^{\&}P$<0.05 compared with AAV-pre-miR-200a-3p+pc-NC group. $\bar{x}\pm s$, n=18.

低(P<0.05); 与AAV-pre-miR-200a-3p+pc-NC组相比, AAV-pre-miR-200a-3p+pc-ALKBH5组小鼠角膜CD31相对荧光强度提高(P<0.05), 见图4与表6。

2.7 各组小鼠角膜中ALKBH5蛋白表达比较

与control组相比, alkali burn组小鼠角膜ALKBH5蛋白表达水平提高(P<0.05); 与AAV-NC组相比, AAV-pre-miR-200a-3p组小鼠角膜ALKBH5蛋白表达水平降低(P<0.05); 与AAV-pre-miR-200a-3p+pc-NC组相比, AAV-pre-miR-200a-3p+pc-ALKBH5组小鼠角膜ALKBH5蛋白表达水平提高(P<0.05), 见图5和表7。

2.8 miR-200a-3p与*ALKBH5*相互关系

如图6所示, Starbase数据库表明miR-200a-3p与*ALKBH5*有互补结合序列。双荧光素酶活性检测结果显示, 与*ALKBH5* WT和miR-NC质粒共转相比, *ALKBH5* WT和miR-200a-3p mimic质粒共转HUVEC细胞, 酶活性降低(P<0.05), 见表8。RIP实验结果显示, 与IgG组相比, Ago2蛋白富集的miR-200a-3p和ALKBH5明显提高(P<0.05), miR-200a-3p和*ALKBH5*具有靶向关系, 见表9。

3 讨论

角膜的缺血和透明特性是维持视力所必需的条件, 急性眼部化学(碱和酸)烧伤会导致严重的并发症和严重的视力丧失; 其中碱的亲脂性更容易穿透角膜, 导致比酸更严重的损伤[11]。角膜新生血管形成可导致角膜混浊和慢性循环炎症, 感染、炎症、缺氧、外伤、角膜变性和角膜移植都会破坏角膜稳态, 促进新生血管形成[12]。目前, 角膜新生血管治疗包括抗炎药和基于抗体的血管内皮生长因子抑制剂, 然而, 其治疗效果较差, 需不断探索新的治疗方法以提高治愈率[13]。

miRNA在眼部新生血管疾病中作为血管生成调节剂一直被广泛研究[14]。研究表明, 血小板来源的miR-200a-3p通过靶向丝裂原活化蛋白激酶14(mitogen-activated protein kinase 14, MAPK14)调节内皮细

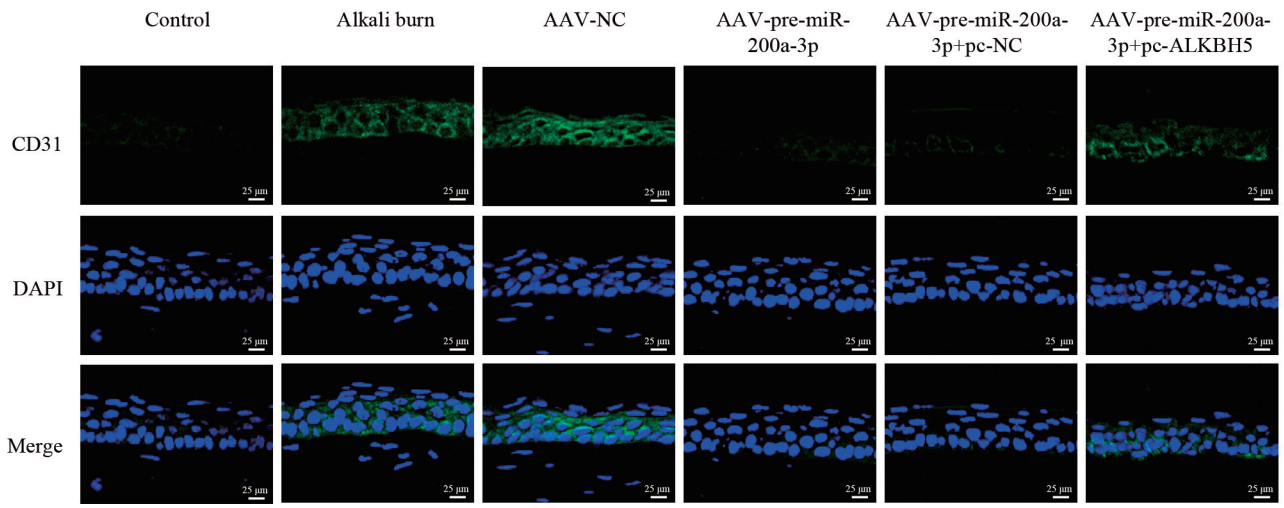

图4 各组小鼠角膜CD31免疫荧光染色

Fig.4 Immunofluorescence staining of CD31 cornea of mice in each group

表6 各组小鼠角膜CD31相对荧光强度比较

Table 6 Comparison of relative fluorescence intensity of CD31 in mouse corneas in each group

分组 Groups	相对荧光强度 Relative fluorescence intensity
Control	1.00±0.11
Alkali burn	2.54±0.32*
AAV-NC	2.57±0.35
AAV-pre-miR-200a-3p	1.38±0.18$^{\#}$
AAV-pre-miR-200a-3p+pc-NC	1.36±0.19
AAV-pre-miR-200a-3p+pc-ALKBH5	2.34±0.29$^{\&}$
F	44.663
P	0.000

*P<0.05, 与control组比较; $^{\#}P$<0.05, 与AAV-NC组比较; $^{\&}P$<0.05, 与AAV-pre-miR-200a-3p+pc-NC组比较。$\bar{x}\pm s$, n=18。

*P<0.05 compared with control group; $^{\#}P$<0.05 compared with AAV-NC group; $^{\&}P$<0.05 compared with AAV-pre-miR-200a-3p+pc-NC group. $\bar{x}\pm s$, n=18.

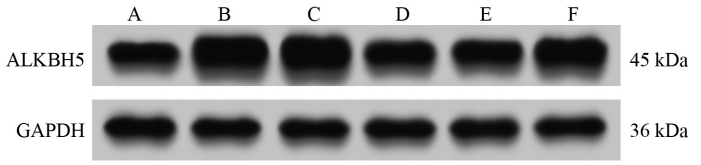

A: control组; B: alkali burn组; C: AAV-NC组; D: AAV-pre-miR-200a-3p组; E: AAV-pre-miR-200a-3p+pc-NC组; F: AAV-pre-miR-200a-3p+pc-ALKBH5组。

A: control group; B: alkali burn group; C: AAV-NC group; D: AAV-pre-miR-200a-3p group; E: AAV-pre-miR-200a-3p+pc-NC group; F: AAV-pre-miR-200a-3p+pc-ALKBH5 group.

图5 各组小鼠角膜中ALKBH5蛋白表达条带

Fig.5 ALKBH5 protein expression bands in the corneas of mice in each group

胞中内皮素1(endothelin-1, ET-1)和VEGFA的表达[15]。CircRNA SCMH1调节miR-200a-3p/锌指E-box结合同源盒蛋白1(zinc finger E-box binding homeobox 1, ZEB1)信号轴, 促进糖尿病诱导的视网膜上皮–间充质转化[16]。在本研究中alkali burn组小鼠角膜混浊, 角膜基质炎症细胞浸润, 胶原结构松弛, 角膜厚度增加, 胶原体积分数、角膜细胞凋亡率及CD31表达水平提高, miR-200a-3p水平降低; 过表达miR-200a-3p

表7 各组小鼠角膜中ALKBH5蛋白表达比较

Table 7 Comparison of ALKBH5 protein expression in the cornea of mice in each group

分组 Groups	ALKBH5
Control	1.05±0.12
Alkali burn	2.36±0.31*
AAV-NC	2.42±0.32
AAV-pre-miR-200a-3p	1.24±0.15$^{\#}$
AAV-pre-miR-200a-3p+pc-NC	1.27±0.16
AAV-pre-miR-200a-3p+pc-ALKBH5	2.32±0.28$^{\&}$
F	45.019
P	0.000

*P<0.05, 与control组比较; $^{\#}P$<0.05, 与AAV-NC组比较; $^{\&}P$<0.05, 与AAV-pre-miR-200a-3p+pc-NC组比较。$\bar{x}\pm s$, n=18。

*P<0.05 compared with control group; $^{\#}P$<0.05 compared with AAV-NC group; $^{\&}P$<0.05 compared with AAV-pre-miR-200a-3p+pc-NC group. $\bar{x}\pm s$, n=18.

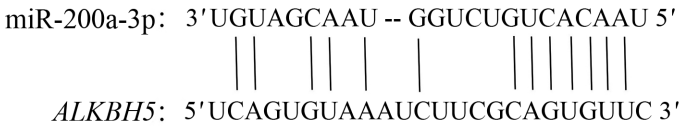

图6 miR-200a-3p与*ALKBH5*靶向结合位点预测

Fig.6 Prediction of targeted binding sites of mir-200a-3p and *ALKBH5*

表8 双荧光素酶活性检测结果

Table 8 Detection results of diluciferase activity

分组 Groups	*ALKBH5* WT	*ALKBH5* MUT
miR-NC	1.06±0.12	1.04±0.11
miR-200a-3p mimic	0.48±0.07	1.03±0.11
t	10.226	0.157
P	0.000	0.878

$\bar{x}\pm s$, n=6.

表9 RIP实验检测miR-200a-3p和*ALKBH5*的靶向关系

Table 9 RIP experiment detected the targeting relationship between miR-200a-3p and *ALKBH5*

分组 Groups	miR-200a-3p	*ALKBH5*
IgG	1.05±0.11	1.02±0.11
Ago2	7.36±0.65	8.21±0.74
t	23.446	23.541
P	0.000	0.000

$\bar{x}\pm s$, n=6.

后, 小鼠角膜混浊与炎症浸润减轻, 角膜厚度减少, 胶原体积分数、角膜细胞凋亡率和CD31表达水平降低。这提示过表达miR-200a-3p对碱烧伤小鼠角膜新生血管生成具有抑制作用。

miRNA通过与靶mRNA的3′非翻译区(3′ untranslated region, 3′ UTR)配对, 在转录后水平上抑制基因表达, 并影响mRNA的稳定性和翻译[17]。本研究采用双荧光素酶活性和RIP实验验证发现, miR-200a-3p与*ALKBH5*存在靶向关系。ALKBH5最近被鉴定为一种内源性m^{6}A去甲基化酶, 与多种生物

过程有关。而m^{6}A是真核RNA中最丰富、动态可逆且进化保守的内部化学修饰，通过前mRNA加工、mRNA衰变和翻译等方式影响RNA代谢，对于在转录后水平调节基因表达至关重要[18]。近年来，ALKBH5被认为是血管生成的重要调控因子，其通过以m^{6}A依赖的方式对*WNT5A* mRNA进行转录后调控并使其稳定性降低，从而在缺血后血管生成中发挥负调控作用[19]。另外，ALKBH5通过蛋白激酶B(protein kinase B, AKT)/哺乳动物雷帕霉素靶蛋白(mammalian target of rapamycin, mTOR)通路导致年龄相关性黄斑变性中的视网膜色素上皮异常和脉络膜新生血管形成[20]。本研究在alkali burn组小鼠中观察到ALKBH5表达水平升高，而过表达miR-200a-3p后，ALKBH5表达下调，且在miR-200a-3p和ALKBH5同时过表达的小鼠角膜组织中，ALKBH5蛋白水平升高，小鼠角膜胶原沉积加重，细胞凋亡增加，血管生成能力增强。由此提示miR-200a-3p可能是通过抑制ALKBH5表达从而抑制碱烧伤小鼠的角膜新生血管生成的。此外，结合参考文献[8]可进行推测，ALKBH5以m^{6}A去甲基化依赖方式稳定*FOXM1*基因的mRNA，提高其蛋白表达，进而通过VEGF等下游因子驱动角膜新生血管形成；miR-200a-3p抑制ALKBH5表达，从而抑制碱烧伤小鼠角膜新生血管生成。

综上所述，miR-200a-3p通过抑制ALKBH5表达抑制碱烧伤小鼠的角膜新生血管生成。角膜碱烧伤后的新生血管形成临床治疗手段有限，且疗效欠佳，本研究提供了未来临床治疗中miRNA靶向治疗的潜在靶点，有助于研究碱烧伤的治疗药物，但本研究仅使用小鼠模型，未进行临床研究，后续研究可基于miR-200a-3p和ALKBH5继续临床研究，此外，本研究未进行多时间点动态观察，后续研究可进行深入探究。

参考文献 (References)

[1] AMMASSAM VEETTIL R, LI W, PFLUGFELDER S C, et al. A mouse model for corneal neovascularization by alkali burn [J]. J Vis Exp, 2023, 30(196): 1-10.

[2] LI Q, HUA X, LI L, et al. AIP1 suppresses neovascularization by inhibiting the NOX4-induced NLRP3/NLRP6 imbalance in a murine corneal alkali burn model [J]. Cell Commun Signal, 2022, 20(1): 1-12.

[3] DENG Q, GAO Y, WANG Y, et al. LSD1 inhibition by tranylcypromine hydrochloride reduces alkali burn-induced corneal neovascularization and ferroptosis by suppressing HIF-1α pathway [J]. Front Pharmacol, 2024, 15(1): 1-19.

[4] CHEN L, LI S, FU Y. MicroRNAs in corneal diseases: emerging roles as biomarkers, regulators, and therapeutics [J]. Ocul Surf, 2025, 38(1): 14-30.

[5] YAŞAR M, ÇAKMAK H, DÜNDAR S, et al. The role of microRNAs in corneal neovascularization and its relation to VEGF [J]. Cutan Ocul Toxicol, 2020, 39(4): 341-7.

[6] XUE L, XIONG C, LI J, et al. miR-200-3p suppresses cell proliferation and reduces apoptosis in diabetic retinopathy via blocking the TGF-β2/Smad pathway[J]. Biosci Rep, 2020, 40(11): 1-12.

[7] LIAO Z, WANG J, XU M, et al. The role of RNA m^{6}A demethylase ALKBH5 in the mechanisms of fibrosis [J]. Front Cell Dev Biol, 2024, 12(1): 1-12.

[8] WANG W, LI H, QIAN Y, et al. ALKBH5 regulates corneal neovascularization by mediating FOXM1 m^{6}A demethylation [J]. Invest Ophthalmol Vis Sci, 2024, 65(12): 1-12.

[9] PENG Y, WANG Q, XU J, et al. P300 promotes RUNX1 transcription to regulate autophagy and drive corneal neovascularization [J]. Invest Ophthalmol Vis Sci, 2025, 66(11): 1-14.

[10] WANG P, HAO P, CHEN X, et al. Targeting HMGB1-NFκB axis and miR-21 by glycyrrhizin: role in amelioration of corneal injury in a mouse model of alkali burn [J]. Front Pharmacol, 2022, 13(1): 1-15.

[11] LI S, SHI S, XIA F, et al. CXCR3 deletion aggravates corneal neovascularization in a corneal alkali-burn model [J]. Exp Eye Res, 2022, 225(1): 109265.

[12] NICHOLAS M P, MYSORE N. Corneal neovascularization [J]. Exp Eye Res, 2021, 202(1): 108363.

[13] VIVANCO-ROJAS O, GARCÍA-BERMÚDEZ M Y, ITURRIAGA-GOYON E, et al. Corneal neovascularization is inhibited with nucleolin-binding aptamer, AS1411 [J]. Exp Eye Res, 2020, 193(1): 107977.

[14] PLASTINO F, PESCE NA, ANDRÉ H. MicroRNAs and the HIF/VEGF axis in ocular neovascular diseases [J]. Acta Ophthalmol, 2021, 99(8): e1255-62.

[15] YANG J, XU H, CHEN K, et al. Platelets-derived miR-200a-3p modulate the expression of ET-1 and VEGFA in endothelial cells by targeting MAPK14 [J]. Front Physiol, 2022, 13(1): 1-13.

[16] HE Y, HOU X T, GUAN Y X, et al. CircRNA SCMH1 regulates the miR-200a-3p/ZEB1 signaling axis to promote diabetes-induced retinal epithelial-mesenchymal transition [J]. Exp Eye Res, 2022, 224(1): 109264.

[17] LI H, LIU Q, ZHANG Q, et al. miR-200a-3p regulates PRKACB and participates in aluminium-induced Tau phosphorylation in PC12 cells [J]. Neurotox Res, 2022, 40(6): 1963-78.

[18] FANG M, YE L, ZHU Y, et al. M^{6}A demethylase ALKBH5 in human diseases: from structure to mechanisms [J]. Biomolecules, 2025, 15(2): 1-23.

[19] ZHANG X, ZHOU L, TIAN C, et al. ALKBH5 in development: decoding the multifaceted roles of m^{6}A demethylation in biological processes [J]. Front Mol Biosci, 2025, 12(1): 1-13.

[20] SUN R X, ZHU H J, ZHANG Y R, et al. ALKBH5 causes retinal pigment epithelium anomalies and choroidal neovascularization in age-related macular degeneration via the AKT/mTOR pathway [J]. Cell Rep, 2023, 42(7): 1-23.